Journal of Building Engineering 69 (2023) 106245

Contents lists available at ScienceDirect

Journal of Building Engineering

journal homepage: www.elsevier.com/locate/jobe

Assessment of the dynamic thermal behaviour of a test room using computer simulations and experimental measurements

Marco Marigo *, Giacomo Tognon, Giulia Alessio, Michele De Carli, Angelo Zarrella

Department of Industrial Engineering - Applied Physics Section, University of Padova, Via Venezia 1, 35131, Italy

ARTICLE INFO

Keywords:
Radiant systems
Building simulation
HVAC
Test room
Indoor environmental quality

ABSTRACT

People spend most of the time indoors and adequate comfort level in buildings is fundamental for their well-being and productivity. These issues can be investigated using both simulation models and experimental measurements in dedicated laboratories or in real buildings. The numerical and experimental approaches need to be combined in order to overcome the limitations of each one. This paper presents the application of a detailed numerical model to the CORE-CARE laboratory built at the University of Padua, a test room employed for indoor environmental quality (IEQ) evaluations. The HVAC plant consists of a mechanical ventilation unit and radiant systems for space heating and cooling. Each radiant surface presents different constructive characteristics and can operate independently. The test room is a novelty in this panorama, as it was integrated in an existing building, as a room for regular use. The impossibility of controlling external disturbances makes the dynamic modelling of the room extremely important, for the laboratory control and knowledge. For this reason, the test room behaviour in response to different HVAC system settings and external disturbances is analysed. Two experimental campaigns were carried out both in the heating and cooling seasons, activating one surface at a time, in order to both validate the model and set-up the transient thermal behaviour of the laboratory. In summer, three experimental set-ups were arranged: closed blinds, opened blinds and presence of a thermal dummy. The data analysis highlights that the North surface exhibits the fastest response in both seasons, whereas the floor is the slowest due to its inertia. In summer, the active surface equilibrium temperature is closer to the water supply temperature for responsive and massive surfaces, and it rises with incoming solar radiation and thermal dummy heat gain. The cooled floor enhances the space's thermal stratification. Simulation results show that the model reproduces the system's real dynamics, with a maximum RMSE of 2.3 and 1.9 °C for the North surface and air temperature.

Nomenclature

C_s	Shading Coefficient [−]
D_{max}	Maximum deviation [°C]
d_{ext}	External diameter of the pipe [mm]
$Grad_{AVG,air}$	Average air temperature gradient during start-up and operation [K/h]
$Grad_{AVG,sur}$	Average surface temperature gradient during start-up [K/h]
$\dot{m}_w$	Water mass flow rate [kg/h]

* Corresponding author.
E-mail address: marco.marigo@unipd.it (M. Marigo).

https://doi.org/10.1016/j.jobe.2023.106245
Received 19 January 2023; Received in revised form 1 March 2023; Accepted 4 March 2023
Available online 7 March 2023

n_t	Number of timesteps [−]
s	Thickness of the pipe [mm]
T	Temperature [°C]
t	Specific timestep [s]
Δh	Height difference between the air temperature sensors [m]
$\Delta T_{sur,w}$	Temperature difference between surface and supply water during operation [K]
ΔT_{vert}	Vertical air temperature gradient [K/m]
Δt	Timestep length [s]
$\Delta \tau_{ON}$	Surface start-up time [minutes]
τ	Time [minutes]

Subscripts

H	Horizontal
m	Measured values
m,avg	Average of the measured values
s	Values from simulations
sur	Surface
supply	Supply water of radiant systems
0.1 m	Sensor at 0.1 m height
1.7 m	Sensor at 1.7 m height

1. Introduction

The importance of people's well-being in indoor environments has been largely studied in the literature. It is widely recognised that people spend most of their time indoors and that the environment's quality affects people's well-being, health, and productivity [1]. According to the analysis carried out by Fisk, these aspects have an economic impact in terms of savings and productivity gains [2]. Moreover, more recent researches focus on the complex correlation of indoor environmental quality and productivity with social, psychological and cultural factors [3]. On the other side, it is essential to consider energy efficiency issues as strictly related to indoor environmental quality (IEQ). The research carried out by Pedersen et al. [4] highlights that occupants rarely associate these two aspects due to the complexity of managing the systems contributing to indoor building conditions. Due to the importance of energy consumption issues, a holistic approach is encouraged in the literature. The most recent update of Eurostat Statistics [5] shows that in European Union, buildings' final energy consumption in 2020, including households, commercial and public services, contributes around 38% to the available energy for final use. In this context, the contribution required to scientific research for analysing interactions between people and the indoor environment is consistent, and this paper aims to contribute to this topic.

Different approaches can be applied to analyse human perceptions and comfort due to the surrounding environment. It is possible to make a general distinction between modelling and experimental approach, but in both cases, the availability of reliable experimental data is essential to obtain realistic results. In this context, the contribution of experimental campaigns in climatic chambers based on measurements and surveys is significant. According to Pisello et al. [6], a test room can be defined as "an enclosed space, environmentally controlled and properly instrumented, in which human-centric comfort studies can be performed through actual occupants' presence and monitoring". Many reviews have been published on this topic: Ganesh et al. collected papers that assess the impact of different factors (visual, acoustic, IAQ and thermal) on room occupants; they highlighted that most of the works found (34%) showed an experimental approach [7]. According to Wu et al., occupants in buildings are affected by multiple factors simultaneously, and chamber tests are the best way to reproduce and analyse their combined effect [8]. Das et al. focused their review on thermal comfort and compared different approaches for its analysis, theoretical models and experimental approaches; they state that in research on thermal comfort, it is essential to have rooms in which conditions can be created and analysed [9]. Concerning theoretical models, Martins et al. give an exhaustive overview of personal models, considering them useful to predict specific thermal requirements, highlighting that all reliable models are built through data collection on office buildings, in most cases reproduced in climatic chambers [10]. On the other side, reviews focus on results from tests in controlled environments, analysing the different methods for carrying out the experiments [11] or investigating the most crucial output for these tests [12]. From the collected articles, it can be deduced that climatic chamber tests have broad applications in IEQ studies: they can be used to analyse the variables' combined effect on occupants and the possibility of controlling each one separately takes to significative results, more reliable than field studies. Many studies use the survey methodology to evaluate the direct impact on people. However, this is not the only output, as models need to be validated with measured data, and for this aspect, the presence of test room experiments is essential. The use of test rooms to contribute to research dealing with comfort issues in indoor spaces is significant, and their use can be extended to new studies based on more complex topics, such as the subjectivity of perception [13].

In literature, some works highlight the importance of a building simulation model aimed at a better knowledge of a controlled environment. Silva et al. built a CFD model validated through the real chamber, and the results showed a good correspondence with the prototype, leading the authors to conclude that the model can be used for model-based designed optimisation [14]. Similarly, Ramezani et al. built and validated a CFD model on the same equipment to improve its thermal behaviour. They analysed airflow

patterns and humidity distribution and formulated different insulation and flow deflector position hypotheses to reach an optimal configuration [15]. Dostál and Ferkl applied a dynamic model to their climatic chamber and simulated a model predictive control system to optimise the switching on and off of actuators for heating and cooling [16]. Although all these models reproduce the behaviour of controlled environments, supported by experimental data, intending to increase the equipment's knowledge and optimise its behaviour, this approach is almost missing in the literature for test rooms used to evaluate indoor conditions and tests on HVAC equipment. Some models can be found, but their application is focused on different aspects. Riederer et al. proposed a zonal model validated in a test room with good results for assessing indoor conditions and HVAC systems behaviour [17]. Also Vidhyashankar et al. compared simulation results obtained by their air-lumped model with experimental data; they plan to use the model in the future to study the optimal control that accounts for both comfort and HVAC system energy consumption [18]. The modelling of test rooms through CFD is an approach also found in some works: in Catalina et al. and Lança et al., the CFD approach is used for predicting airflows and thermal performances of particular system settings (cooled ceiling and ventilation during day and night cooling strategies). Both models are very detailed and supported by experimental data, and results agree with their work's purpose, but they require high computational time [19,20]. A similar approach can be found in Dong et al., but the aim is to evaluate comfort due to different solar radiation levels in a room heated with floor heating; they simulated three different cases, with solar radiation, without radiation and with shaded radiation and concluded that its influence is significant for thermal comfort evaluation [21]. Bonello et al. built a CFD model based on measurements on a test room for the study of humidity distribution in indoor environment [22]. A different approach is shown by Derakhtenjani and Athienitis in their paper. They modelled their test room with a model based on transfer functions to evaluate the thermal response and derive considerations concerning energy efficiency. They also consider the thermal mass of surfaces and the time delay between radiant floor input and air temperature variations inside the room [23]. Finally, Dongellini et al. present a test room for heat pump testing. In their paper they showed the development of different models based on collected data (Trnsys, Matlab-Simulink and STAR-CCM+) and highlighted the importance of a coupled experimental-modelling approach aimed at contributing in the design phase, the definition of the system operative range and the analysis of the effective equipment behaviour in dynamic conditions [24].

The research on radiant panels is rising in importance in the recent literature thanks to the possibility of testing their performance in controlled rooms. Multiple approaches are used for the analysis of these systems: the availability of experimental data is often used for the calculation of real panels' performance, but in many works, measurements are used for the calibration of models successively applied for further analysis. Detailed computational models are often used for both evaluating the thermal environment and solving the temperature distribution in the radiant system, but they are suitable for steady-state simulations given the high computational costs. Instead, simplified numerical models (e.g., RC models) can describe the dynamics of the radiant systems and are promising for integration in transient building energy simulation. A review of the modelling techniques for radiant cooling systems is provided by Hassan and Abdelaziz [25].

In this context, different purposes can be outlined in the recent studies focused on radiant panels. The first group of papers is characterised by analysing conventional panels' performance. The heat transfer coefficient is one of the most used parameters to evaluate panels' thermal behaviour and many works report this approach [26]. Koca focused his attention on evaluating heat transfer coefficients of radiant wall cooling systems in a test room at varying supply water temperatures [27]. A similar approach is proposed by Yuan et al. for calculating the heat transfer coefficient of a ceiling radiant cooling panel [28]. Another important topic is the problem of condensation in cooling conditions. Jin et al. analysed the variations of surface temperature in traditional metal panels at different supply water temperatures and flow rates and in different indoor conditions defining limits for avoiding condensation and asserting that the indoor temperature, the average temperature of the non-cooling surface and the temperature of the inner surface of the outer window have an important contribution to surface temperature of the radiant ceiling panel [29]. Many works focus their analysis on steady-state models and experimental conditions: Yu et al. studied the variation of the equivalent radiant system resistance depending on tubes spacing and aluminum foil thickness [30]; Yu et al. showed a correlation between supply temperature and both surface temperature and heating-cooling capacity in steady-state conditions. However, as they proposed a light floor panel, they highlighted the importance of performing a dynamic analysis studying its behaviour in the start-up phase and concluding that the light floor panel shows high responsiveness, being 30 min faster than a traditional one [31].

The second group of papers proposes radiant systems with particular layout, geometry, or material and tests the solution in controlled chambers. Krajcik et al., in their paper, analysed a radiant system with pipes attached to low-conductivity aerated bricks. They studied the dynamic behaviour of the panel, finding that the thermal response was fast despite the coupling of the pipe with the bricks; they also observed a small difference between water and average surface temperature but a not uniform temperature compared to wall embedded systems [32]. Another kind of panel with a segmented and concave surface was proposed. Tests were performed to define the panel's performance, with changing water flow rates and supply temperatures in both steady-state and dynamic tests. The parametric analysis showed a higher impact on inlet water temperature than on flow rate; however, the cases with a higher flow rate and lower inlet water temperature always had higher time constant values [33]. The same authors also validated a CFD model with experimental data and optimised the geometrical parameters, using thermal comfort parameters as targets [34]. The analysis of radiant systems' performance for their use in buildings' retrofit actions is another topic widely reflected in the literature. In particular, Junasová et al. validated a dynamic model of a radiant system with experimental data. They modified some parameters obtaining different configurations applicable in retrofit actions and performing a sensitivity analysis to define the effect of construction parameters on the systems' thermal performance [35]. A contribution to the selection of the radiant system typology is given by Oravec et al. They performed a comparative study between six radiant solutions based on dynamic simulations, comparing the different solutions in dimensioning parameters, thermal performance, applicability to retrofit actions and costs. They aim to guide designers in choosing the most appropriate solution in each case [36].

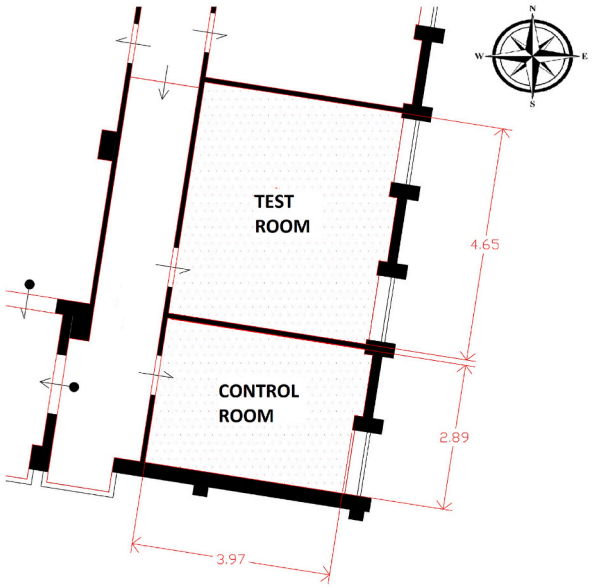

Fig. 1. Plan view of the CORE-CARE laboratory (4.65 m × 3.97 m).

1.1. Novelty and aim of the paper

In this paper, a dynamic thermal model is applied to the CORE-CARE laboratory, a test room dedicated to experimental investigations on IEQ analyses in moderate environments. Most existent test rooms used for research activities are often small spaces assembled inside another larger room whose indoor parameters can be altered and controlled over time, simulating external disturbances, such as outdoor temperature and solar radiation. This means that these test rooms are subjected to set boundary conditions that can be regulated by the operator. The CORE-CARE laboratory represents a novelty in this panorama since it is directly integrated with an existing building as it was a room for regular use. This characteristic makes it an interesting tool to conduct tests on IEQ aspects with occupants under real external disturbances, which are uncontrollable and variable over time. In this way, the experimental settings would represent real-life situations. The laboratory is equipped with a mechanical ventilation unit and independent radiant systems for each surface to have different surface temperatures.

In this context, the impossibility of controlling external disturbances makes the analysis of the test room thermal performance and its modelling extremely important to observe how the indoor parameters are affected by unfixed boundary conditions. Considering the particular configuration of the laboratory, dedicated experimental measurements are carried out both in the cooling and heating season to point out its dynamics and thermal response to different disturbs. With the collected data, the numerical model is built with the DigiThon software [37] to have a tool for predicting the room thermal behaviour under different test settings. This article sets up a procedure for the assessment of the laboratory in transient conditions and also provides a further validation of the DigiThon model for future works in the test room.

2. Description of the CORE-CARE laboratory

The CORE-CARE laboratory (COntrolled room for building Environmental Comfort Assessment and subjective human Response Evaluation) is a test room built at the Department of Industrial Engineering of the University of Padova (Italy). The opportunity to test different environmental conditions, controlling each parameter independently, and study how thermal comfort, indoor air quality (IAQ), acoustics and lighting affect occupant well-being may lead the laboratory to play an essential role in future scientific production concerning indoor environmental quality (IEQ) issues. In particular, the possibility of studying the effect of building characteristics and HVAC systems settings on occupants' well-being, comfort and productivity was one of the aims of the laboratory construction.

2.1. Position and layout

The laboratory is on the third floor of the Department of Industrial Engineering at the University of Padova. It was built by refurbishing a space previously used as a meeting room. For this reason, one of CORE-CARE's attractive aspects is its integration with an existing building: it is not a controlled room built within an indoor space; instead, it is part of it and has characteristics similar to a frequently used room. One of the vertical walls faces the external environment and two windows are installed; the ceiling borders the roof, whereas all the other surfaces are adjacent to heated rooms or a corridor. The laboratory consists of a test room, where the experiments occur, and a control room, where the HVAC and monitoring systems are controlled. The test room has a floor area of 18.5 m^2 and the room height is 2.8 m; the glazed surface is 3.4 m^2. In Fig. 1, the representation of the laboratory layout is shown.

All the test room surfaces are equipped with radiant systems: they were placed over the pre-existing walls and given by different manufacturers. For this reason, each laboratory surface has different construction features, taking to different behaviour during its

Table 1
Characteristics of the radiant panels installed in the CORE-CARE test room.

	Tubes dimensions (d_{ext} x s)	Number of circuits	Panel's thickness over tubes	Active surface	Pitch	Tubes length per active area
	[mm x mm]	[−]	[mm]	[m^2]	[cm]	[m/m^2]
Floor	10.5 × 1.25	5	9.5	17.66	8.3	12.0
Ceiling	10.5 × 1.25	9	12.5	12.96	7.6	13.2
East Wall	8.0 × 1.0	5	7.0	6.00	5.0	17.6
North Wall	10.0 × 1.3	6	15.0	7.20	4.3	23.3
South Wall	9.9 × 1.1	6	15.0	7.50	7.8	12.9
West Wall	10.1 × 1.1	4	4.9	4.80	6.0	16.7

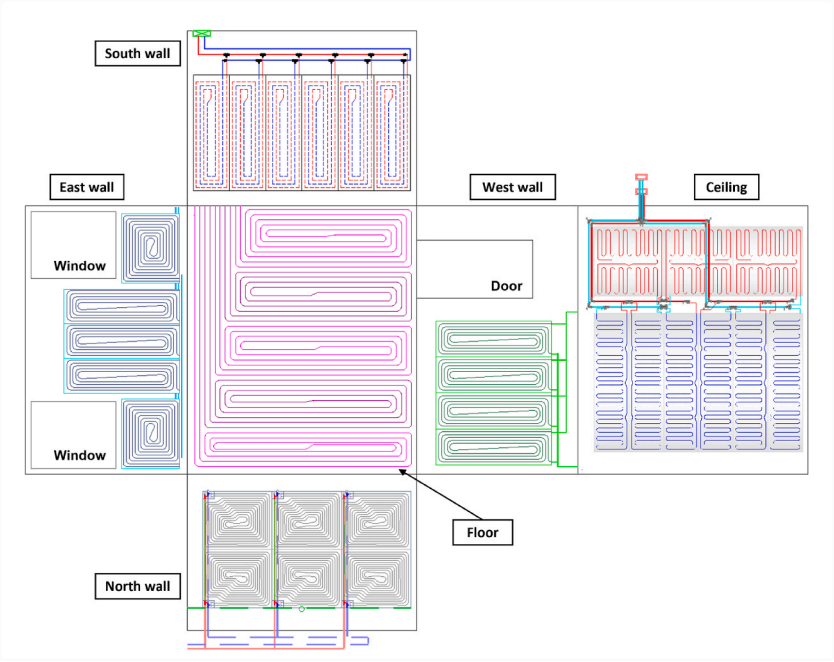

Fig. 2. Layout of the panels installed on the different surfaces.

operations. Before the radiant panels' installation, an insulation layer was placed between the building structure and the active panel, avoiding thermal heat dispersions towards adjacent environments; as the external wall was already provided with its insulation panel, the application of a further layer led to a very low transmittance wall. Concerning the floor, the pipes are embedded in a thermal diffusion layer (quartzite resin screed) between studs, with 9.5 mm thickness over the tubes; in all the other surfaces, prefabricated plasterboard panels with built-in pipes are placed over the insulation layer. Except for the floor, all the other surfaces are similar; the only differences concern plasterboard or insulation thickness and the layout of the pipes. In Table 1, the characteristics of each radiant panel are presented; the highlighted tubes' dimensions are the pipe's external diameter and thickness, whereas the density of the tubes is given by the ratio between their length and the active surface of the panel. Finally, the different panels' layout is shown in Fig. 2.

In the pre-existing room, two windows were placed on the East-facing wall that borders the outside. When the test room was built, it was decided to keep the two external windows and place two additional ones flush with the internal wall. The external windows are double glass with an aluminium frame, whereas the recently installed windows are double glass (6 mm thickness each), with a 16 mm gap filled with argon; the frame material is PVC and their dimensions are 1.96 m × 1.38 m each. The thermal transmittance of new windows is 1.17 W/(m^2 K). In the space between the two windows, a venetian blind is placed with slats set at different angles so that the amount of natural light entering from outside can be customised. The stratigraphy of the walls is reported in Appendix A (Table A1-A6).

2.2. HVAC systems

The radiant panels can operate in heating or cooling mode, as they can be supplied with hot or cold water as needed. The water heating and cooling processes occur in the control room, where the HVAC systems are installed. Moreover, a ventilation unit operating with external air is installed, which can work in cooling or heating back-up, dehumidification or free-cooling modes.

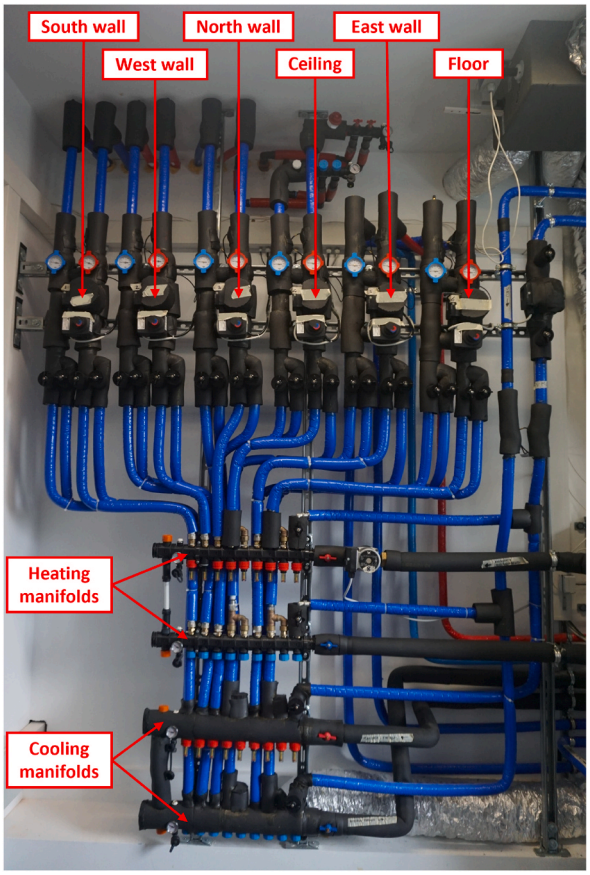

Fig. 3. Manifolds and mixing units of the heating and cooling hydronic circuits.

Fig. 4. Cooling (left) and heating (right) tanks.

2.2.1. *Hydronic circuit*

As already shown in Table 1 and Fig. 2, the four-wall and ceiling radiant systems consist of combinations of panels of different sizes and shapes. All the panels are connected in parallel through a pipe linking each supply and return to the secondary circuit. Similarly, five circuits in the radiant floor system, connected in parallel, constitute the active surface. All the radiant systems are supplied with water from six secondary circuits, each with a dedicated mixing and pumping unit. The secondary circuits flow into modular manifolds connected to the heating and cooling primary circuit. In Fig. 3, the layout of the water distribution system is shown with the mixing units controlling the supply water temperature for each surface.

In the control room, two tanks were installed for hot and cold water production. The hot tank's capacity is 200 L, and the water is heated by three electrical resistances of 1.5 kW each. The three heating elements switch on independently according to a set-point

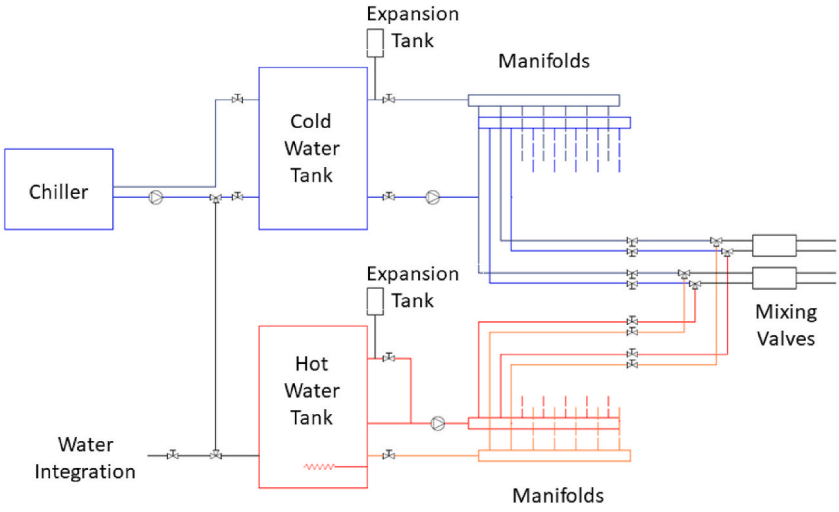

Fig. 5. Hydronic circuit scheme.

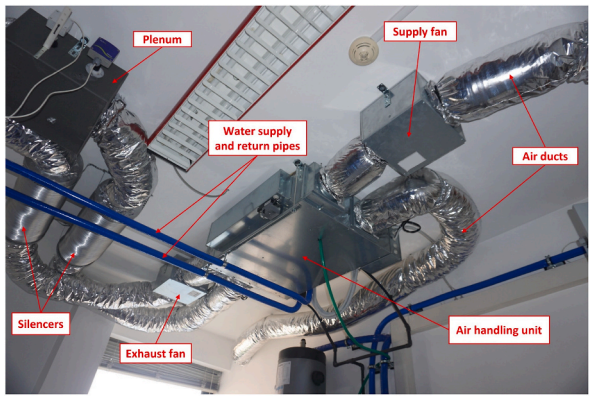

Fig. 6. Mechanical ventilation system's components.

temperature fixed for the tank, which is 45 °C. The cold tank has a capacity of 100 L and is cooled down by a chiller placed on the roof. A plate heat exchanger decouples the cooling and chiller circuits; in analogy with the heating boiler, also in the cooling circuit, the tank has a set-point temperature equal to 10 °C. The chiller presents a cooling capacity of 4.3 kW. In Fig. 4, the heating and cooling systems pictures are provided, whereas in Fig. 5, the scheme of the hydronic circuit is reported.

The temperature control inside the test room is carried out from the control room; therefore, occupants cannot modify the operations of the HVAC systems. The control is carried out by setting the supply temperature for each panel; accordingly, the mixing unit controls the position of a thermostatic valve which mixes the water from the primary circuit with that returning from the panels. A PID controller drives the process.

The only limit for the supply temperature is given by the water set-point temperatures in the two tanks; for this reason, it is possible to work in heating and cooling mode between 10 °C and 45 °C. The hydronic system was built to keep the radiant surfaces independent of each other; therefore, it is possible to set a different supply temperature for the different laboratory surfaces and work in different (heating or cooling) modes with different surfaces simultaneously.

2.2.2. *Ventilation system*

The mechanical ventilation system in the control room consists of a primary air unit for the renewal of ambient air, as shown in Fig. 6.

The ventilation unit can be set in five operation modes: only fresh air, heating and cooling integration, dehumidification and free cooling. In the case of fresh air inlet, air moves through a high-efficiency crossflow heat exchanger before being supplied to the laboratory. In the dehumidification and integration modes, air transformations are performed by a built-in reversible heat pump. The air handling unit is equipped with a water coil connected to the hydronic circuit, contributing to the integration mode in the sensible heat to be released or absorbed by the air.

The AHU allows the control of the supply and extraction air flow rate, which lies between 80 m^3/h and 250 m^3/h. Regarding air

change rate, the flow rates lie between 1.8 h^{-1} and 5.7 h^{-1}. The machine gives the possibility of setting the inlet air temperature, with a range that varies according to the season of operation: in heating mode, the supply temperature can be set between 20 °C and 45 °C; in cooling mode, the possible range is between 15 °C and 25 °C. The dehumidification mode can be controlled manually and switched on or off during the cooling season.

Similar to the hydronic system, the control of the ventilating unit can not be performed by the laboratory's occupants and must be carried out by the control room.

2.3. Monitoring system

The monitoring system installed in CORE-CARE consists of 38 sensors in both the control and test rooms. The sensors are connected to the acquisition system, which measures and stores data with 2 s timestep. The following probes installed in the test room aim to measure the environmental parameters of the test room:

- 24 sensors for the measurement of the surface temperature of the six opaque surfaces of the test room;
- 2 sensors for the measurement of the surface temperature of the two glazed surfaces of the test room;
- 3 sensors for measuring the air temperature, located on the vertical column positioned in the centre of the room at three different heights (0.1 m, 0.60 m and 1.70 m);
- 1 sensor located on the vertical column at the height of 1.1 m;
- 3 sensors located in the supply, extraction and external channel of airflow in the ventilation unit;
- 1 sensor to assess the CO_2 level inside the room;
- 3 sensors to assess the CO_2 in supply, extraction and external channel of airflow in the ventilation unit;
- 1 sensor for measuring mean radiant temperature, placed on the column at 0.6 m.

The characteristics of the sensors are given below:

- The surface and air temperature sensors are platinum thermistors, their tolerance is defined as Class F 0,15 (according to Ref. [38]) and the measurement range is between −50 °C and 300 °C.
- The air temperature and relative humidity sensor has 1.5% tolerance in the RH and 0.1 °C in the temperature reading; the measurement range covers all the spectrum for RH and is between −40 °C and 105 °C for the temperature.
- The CO_2 concentration sensor is a Non-Dispersive Infrared sensor; it has absolute tolerance of 30 ppm and the measurement range is between 0 and 10000 ppm.
- The mean radiant temperature sensor is a globe thermometer with 0.2 °C accuracy and measurement range between −30 °C and 70 °C.

3. Analysis of the thermal behaviour of the test room

In this section, the method for the analysis of the thermal behaviour of the CORE-CARE laboratory is presented. The test room is directly integrated with the existing facility, so external disturbances related to climate conditions cannot be controlled and directly impact the laboratory's overall energy balance. Considering this peculiarity, thermal characterisation is fundamental to observing how indoor parameters are affected by unfixed boundary conditions. This first operation was accomplished through a measurements campaign. For this purpose, experimental tests were arranged to provoke different solicitations to the test room. Surface and air temperatures were continuously monitored, determining the thermal response of the laboratory in the different situations it underwent.

On the other hand, building a model that could simulate CORE-CARE's thermal behaviour is crucial to carry out a predictive analysis that could help set future tests. DigiThon was chosen as the tool for carrying out the modelling operation. It was available as it was previously developed by the Authors' research group and has already been validated in different works [37,39,40]. Moreover, its high level of detail and flexibility in analysing radiant panels made it suitable for the aim.

Considering experimental tests with real occupants as the most challenging horizon to exploit the peculiarities of CORE-CARE laboratory, the analysis of the test room responses to the different HVAC systems settings is significant. In a room where all radiant panels have different characteristics and where there is the possibility of working with both radiant and ventilation systems, these coupling of measured data and simulations can give a contribution to investigating some critical factors to reach a good knowledge of the laboratory, also allowing the most precise control possible in the management of the plants.

3.1. Experimental campaign

Different tests were performed for the characterisation during the summer and winter seasons; the same procedure was used in each test. The tests in heating conditions were carried out between 17/10/2020 and 10/11/2020, whereas those in cooling conditions were between 15/06/2021 and 10/08/2021.

Each test presented the same structure, which can be outlined in 4 steps:

- Step 1: Preparation, which consisted of switching on the systems for hot and cold water production, for starting the test with tanks' temperatures set by the user.
- Step 2: Switching on the circulation pumps of the panel.
- Step 3: The circulation pump is switched off after an unfixed time interval, which is needed for reaching and maintaining steady conditions.

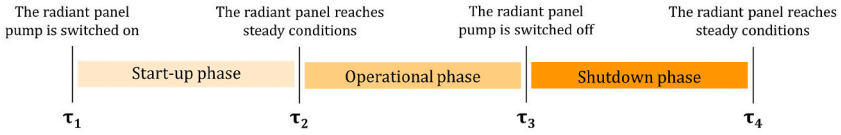

Fig. 7. Key timing and phases of the test. Steady conditions are defined as when temperature difference between following timesteps is lower than 0.1 °C.

- Step 4: The water production and the acquisition systems are switched off. The test is over.

The lengths of the test were slightly different between cooling and heating conditions: for winter tests, it was decided to start circulating hot water during the afternoon and keeping the circuit on during the night; conversely, for summer tests, it was decided to start the tests in the morning and to conclude them in the late afternoon. This approach was justified by the search for the most critical daytime for the system operation for each operation period. Each test was performed with only one active surface to evaluate its behaviour independently. The ventilation unit was used during the cooling tests to avoid condensation over the cooled surfaces. During the tests, the door adjacent to the corridor and the outdoor windows were clearly closed.

The following tests were performed:

- Tests in heating conditions (Test H): Apart from the floor, each surface was tested in heating mode; the supply water temperature ranged between 35 °C and 42 °C, according to the tested surface. The different supply temperatures were chosen to try to keep the same air temperature inside the room. The venetian blinds were closed during all the tests, avoiding direct solar radiation entering the laboratory.
- Tests in cooling conditions with closed blinds (Test C1): Each surface was tested in this series of tests. The water supply temperature was kept constant at 16 °C, and the closed blinds minimised the direct solar radiation entering the room.
- Tests in cooling conditions with open blinds (Test C2): The same setting as the previous test was kept, except for the blind position, whose open position allowed the solar radiation to enter the test room.
- Tests in cooling conditions with internal load (Test C3): During this test series carried out similarly to Test C2, a thermal dummy built up according to European Standard EN 14240:2004 [41] was put in the room. The thermal load associated with the dummy use is 180 W.

3.2. Method for measurements analysis

The analysis of the experimental campaign was carried out through the definition of specific parameters used to study the response of the test room to the different thermal loads provided during the tests.

As a first stage, each test has been divided into three parts: start-up, operation, and shutdown. The test layout and the switching time between the different phases is shown in Fig. 7.

The parameters used for the analysis of measurements are reported in hereafter, along with the corresponding equations for their calculation (Eqs. (1)–(6)):

- Surface start-up time, expressed in minutes

$$\Delta\tau_{ON} = \tau_2 - \tau_1 \tag{1}$$

- Average surface temperature gradient during start-up in [K/h]

$$Grad_{AVG,sur} = \frac{\sum_{t=\tau_1}^{\tau_2} |T_{sur}(t+\Delta t) - T_{sur}(t)|}{n_t \bullet \Delta t} \tag{2}$$

- Average air temperature gradient during start-up and operation in [K/h]

$$Grad_{AVG,air} = \frac{\sum_{t=\tau_1}^{\tau_3} |T_{air}(t+\Delta t) - T_{air}(t)|}{n_t \bullet \Delta t} \tag{3}$$

- Temperature difference between surface and supply water during operation [K]

$$\Delta T_{sur,w} = \frac{\sum_{t=\tau_2}^{\tau_3} |T_{sur}(t) - T_{w,supply}|}{n_t} \tag{4}$$

- Vertical air temperature gradient in [K/m]

$$\Delta T_{vert} = \frac{Max\left(T_{air,1.7\ m} - T_{air,0.1\ m}\right)}{\Delta h} \tag{5}$$

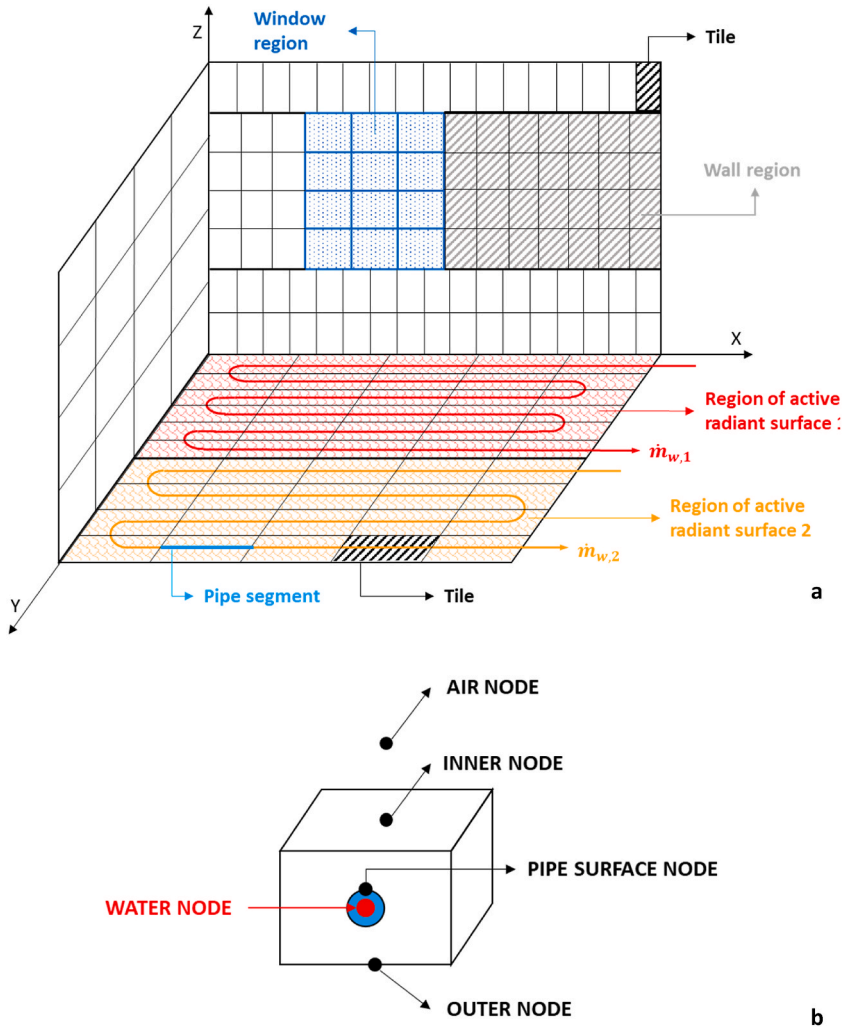

Fig. 8. Room discretisation with DigiThon (a) and detail of a tile representing a generic building element embedding pipes (b).

- Surface temperature variation after start-up [K]

$$Delta = |T_{sur}(\tau_1) - T_{sur}(\tau_2)| \tag{6}$$

3.3. DigiThon modelling

Next to the experimental data's direct analysis, they were compared with the results of dynamic simulations performed with the software DigiThon. A model of the test room was built, and each test session was simulated by imposing different boundary conditions corresponding to disturbances and systems settings that occurred during tests. The modelling approach is exposed in this section, including the simulation settings and the applied boundary conditions.

3.3.1. DigiThon

DigiThon is a model used for energy simulations of multi-room buildings. It is based on the room heat balance using the thermal response factor, as explained in Ref. [42]. Its structure, validation and former application are explained in detail in Refs. [37,39,40].

In the model, the air is considered well-mixed; therefore, only one thermal node represents the air volume inside the room. Conversely, the surfaces present a discretisation through the division into regions which are differentiated between active regions corresponding to radiant panels and inactive regions corresponding to portions of the floor, walls and ceiling without radiant circuits beneath. Each region is further subdivided into elements called "tiles". Fig. 8(a) shows an example of discretising a room with a radiant floor system, where window and wall regions represent inactive surfaces.

Each tile presents different thermal nodes that are used for the thermal balance of the room: there are wall surface nodes, both on the inner and outer side of the element, pipe surface nodes, placed at the surface of each segment, subdividing a pipe making up the radiant system and water nodes, placed in correspondence of the pipe axis, which represent the water temperature; the flow regime inside the pipes is considered to calculate the convective heat transfer fluid between the fluid and wall pipe. For each thermal node, the

Table 2
Shading coefficient (C_s) used in the simulations.

Tested surface	Test H	Test C1	Test C2	Test C3
Floor	0.2	0.5	0.9	0.4
Ceiling	0.2	0.4	0.8	0.4
North Wall	0.2	0.3	0.4	0.4
West Wall	0.2	0.4	0.5	0.4
East wall	0.2	0.3	0.4	0.4
South Wall	0.2	0.4	0.6	0.4

Table 3
Start-up time, average surface gradient, initial temperature, average air gradient and Delta in cooling tests.

	Test C1		Test C2		Test C3	
Tested surface	$\Delta\tau_{ON}$ *(in minutes)*	$Grad_{AVG,sur}$ [K/h]	$\Delta\tau_{ON}$ *(in minutes)*	$Grad_{AVG,sur}$ [K/h]	$\Delta\tau_{ON}$ *(in minutes)*	$Grad_{AVG,sur}$ [K/h]
Floor	100	−4.4	130	−5.0	150	−4.4
Ceiling	120	−3.9	130	−4.3	70	−5.8
North Wall	50	−12.4	60	−11.7	60	−10.9
West Wall	60	−10.0	60	−10.4	60	−9.4
East wall	100	−4.4	60	−8.1	60	−7.3
South Wall	120	−6.4	110	−5.4	90	−6.0
Tested surface	**$T(\tau_1)$ [°C]**	**$Grad_{AVG,air}$ [K/h]**	**$T(\tau_1)$ [°C]**	**$Grad_{AVG,air}$ [K/h]**	**$T(\tau_1)$ [°C]**	**$Grad_{AVG,air}$ [K/h]**
Floor	27.4	−0.9	29.8	−1.1	29.4	−0.9
Ceiling	28.0	−0.7	30.3	−0.9	29.7	−0.5
North Wall	28.6	−0.4	30.8	−0.8	29.7	−0.5
West Wall	29	−0.4	29.6	−0.5	29.0	−0.2
East wall	27.5	−0.3	29.2	−0.5	28.0	−0.3
South Wall	30.5	−0.6	30.3	−0.6	30.1	−0.4
Tested surface	**Delta [°C]**		**Delta [°C]**		**Delta [°C]**	
Floor	9.3		10.9		10.0	
Ceiling	7.9		9.2		6.8	
North Wall	10.5		11.8		10.6	
West Wall	10.1		10.4		9.9	
East wall	7.4		8.3		7.3	
South Wall	10.0		10.0		9.0	

heat balance equation is written obtaining a linear system of equations that can be solved. Fig. 8(b) depicts the thermal nodes of a tile representing a building element with embedded pipes. The model does not consider the effect of the thermal bridges inside the room.

The model performs dynamic simulations of the chosen environment, and the thermal balance is calculated at each timestep. As for the conduction heat transfer through the walls was calculated through the thermal response factors; in this work, they were calculated using the software HEAT2, using the finite difference method technique [43], based on the real walls' stratigraphy (Table A1-A6).

3.3.2. Simulations assumptions and boundary conditions

All simulations were performed under dynamic conditions, each with a length matching that of the corresponding test. The timestep used for simulations is equal to 10 min.

The model geometry and the radiant panel configuration were assumed according to the real geometry of the room. As for the internal heat transfer calculation, the surface convective heat transfer coefficient values were assumed from Standard EN 6946:2017 [44] and kept constant: for vertical walls a value of 2.5 W/(m^2 K) was set, whereas for ceiling and floor two values of 0.7 and 5.0 W/(m^2 K) were assumed, respectively. The software calculates the radiative heat transfer according to the surface temperatures and corresponding view factors.

Some assumptions were taken in the modelling process of the test room. When the internal load was inserted, it was assumed that the partition consisted of 60% convective and 40% radiative gain. Different values of the shading coefficient (C_s) were used as input in the simulations (Table 2), due to each test's different conditions and the variability of meteorological conditions.

The following boundary conditions were set for the simulations:

- The temperature of adjacent internal environments was measured for the whole test period and this value has been used as a boundary condition for the simulations.
- The external climatic conditions were set according to measurements by the Regional Agency of Environmental Protection of Veneto (ARPAV) [45] in the more proximate weather station. The values of the external air temperature, external relative humidity, direct normal radiation, and horizontal diffuse radiation were used as boundary conditions.

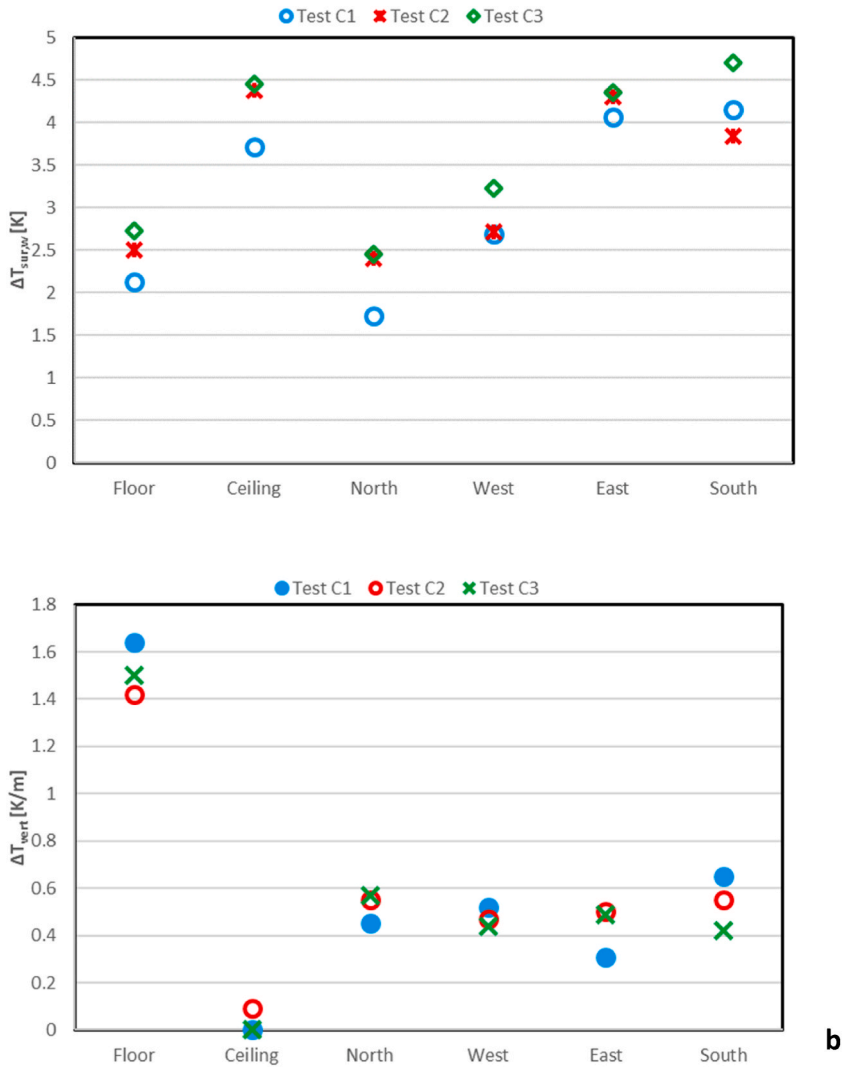

Fig. 9. Temperature difference between surface and supply water (a) and Air stratification - temperature difference between 0.1 m and 1.7 m - (b) in different cooling tests.

In the simulations performed for the heating season, it was decided to consider only the diffuse radiation and neglect the direct component as, on winter days, the low solar height and the shading of the surrounding building do not allow direct radiation to enter the laboratory through windows.

The operations of the HVAC systems were modelled assuming the water flow rate inside the tubes in each radiant panel. The values of the water flow are 100 kg/h for the floor, 78 kg/h for the ceiling, 117 kg/h for the North wall, 150 kg/h for the West wall, 120 kg/h for the East wall, 117 kg/h for the South wall.

The supply water temperature set during the tests was also used as input.

4. Results and discussion

The following paragraphs present measurements and simulation results for heating and cooling seasons. In Section 4.1, the results of the experimental approach are reported, highlighting the thermal behaviour of radiant panels to check the response of the test room to different heating and cooling loads. In section 4.2, the simulation results show the search for a modelling representation of the laboratory for its assessment in future tests. Finally, in Section 4.3, the discussion of the results is carried out.

4.1. Results of the experimental campaign

In Table 3, the velocity of each radiant panel reaching stable conditions, i.e., a temperature difference between consecutive timesteps lower than 0.1 °C, is shown by both start-up time ($\Delta\tau_{ON}$) and average surface temperature gradient in cooling conditions ($Grad_{AVG,s}$). The results highlight that the different layout of the radiant systems leads to differences in reaching the steady condition

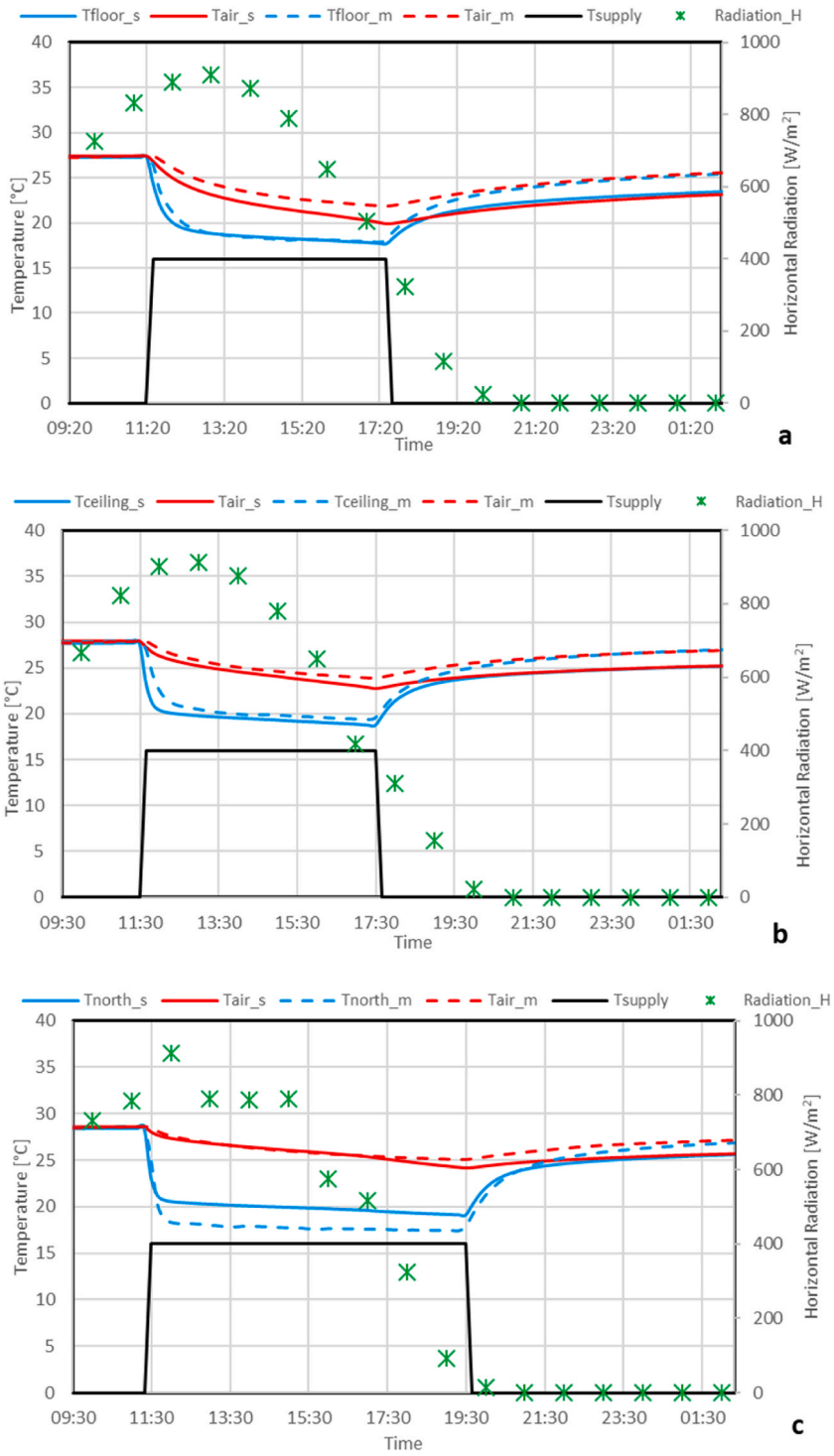

Fig. 10. Average surface temperature detected on the active surface and average air temperature compared to simulation outputs in the cooling tests with closed blinds (Test C1) for the floor, ceiling and north wall.

and those applied in North and West facing walls result in the fastest surfaces. The slowest surface is the floor, which is related to its embedded layout and more massive structure.

The air temperature gradient during the test (start-up and operation phases) was chosen as another representative parameter, and it is reported together with the initial test temperature in the middle part of Table 3. In this case, the surface which influences the air temperature most is the floor, but the ceiling also takes to significant temperature decreases. West and East surfaces seem to have less

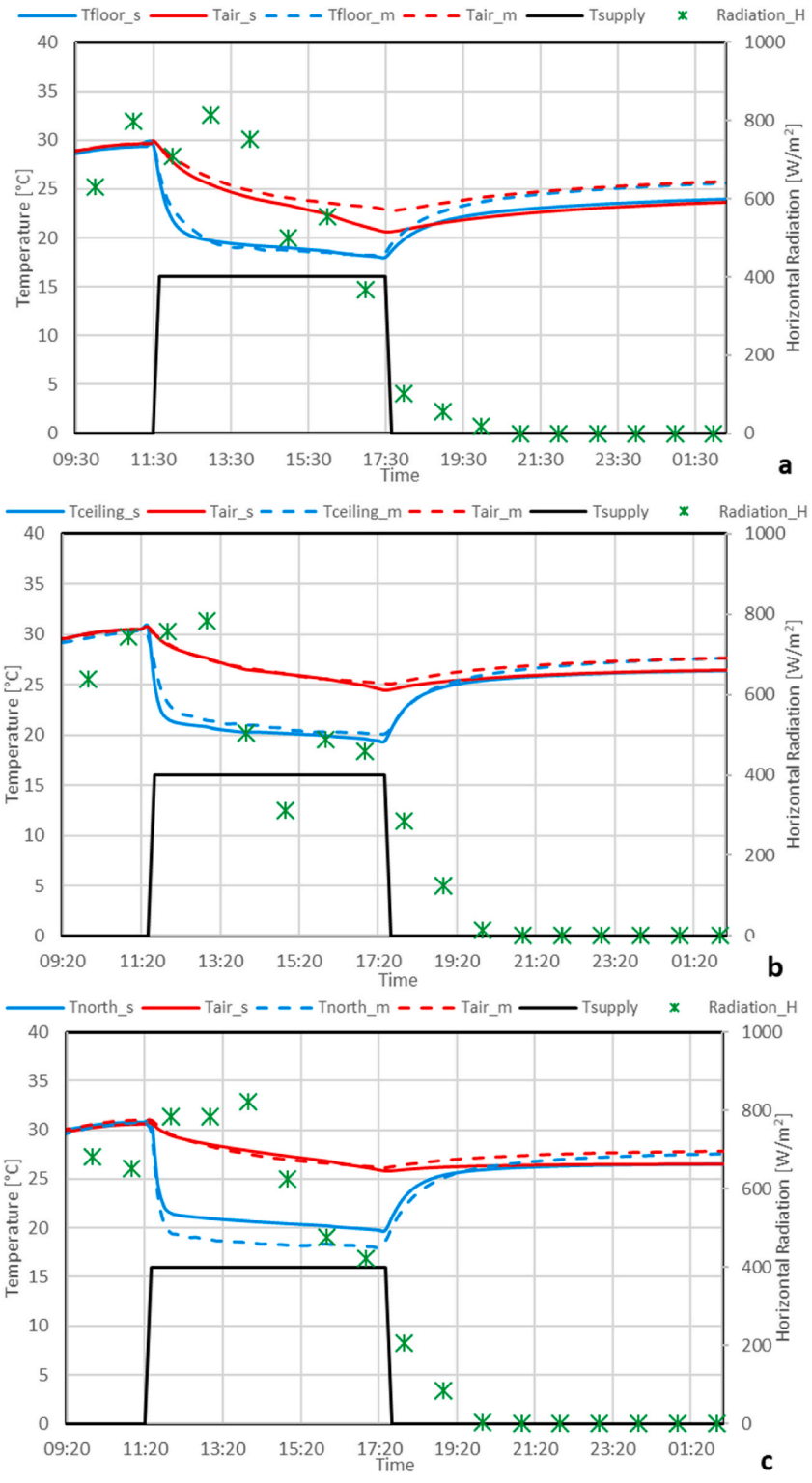

Fig. 11. Average surface temperature detected on the active surface and average air temperature compared to simulation outputs in the cooling tests with open blinds (Test C2) for the floor, ceiling and north wall.

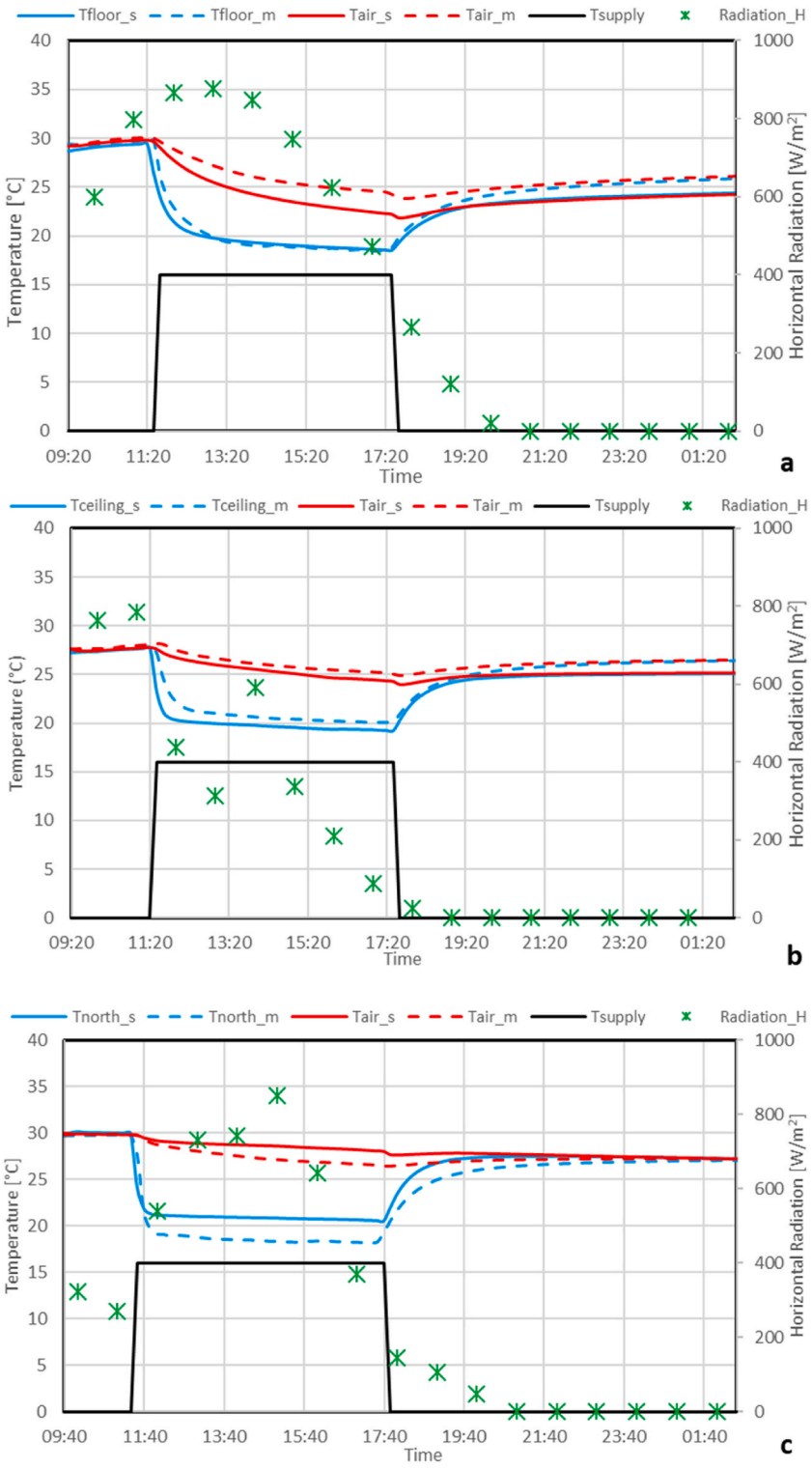

Fig. 12. Average surface temperature detected on the active surface and average air temperature compared to simulation outputs in the cooling tests with heat gain (Test C3) for the floor, ceiling and north wall.

impact on air temperature than North and South walls.

In the last part of Table 3, the surface temperature drop during the start-up phase is highlighted; it depends on the initial temperature of the test, but it is also typical for each wall, with higher values for surfaces that can reach a temperature closer to the supply

Table 4
RMSE and maximum deviation for the average surface and air temperature in cooling tests.

	Test C1		Test C2		Test C3	
Surface Temperature						
Tested surface	**RMSE [°C]**	**D_{max} [°C]**	**RMSE [°C]**	**D_{max} [°C]**	**RMSE [°C]**	**D_{max} [°C]**
Floor	0.5	−2.0	0.5	1.2	0.6	2.1
Ceiling	1.1	3.7	0.8	2.1	1.3	4.0
North Wall	2.0	2.3	2.0	2.3	2.3	−3.5
West Wall	1.4	−2.2	1.8	3.7	1.6	−4.3
East wall	0.8	−2.7	1.1	1.4	0.9	1.0
South Wall	0.7	−1.3	1.6	−2.0	1.2	−1.9
Air Temperature						
Tested surface	**RMSE [°C]**	**D_{max} [°C]**	**RMSE [°C]**	**D_{max} [°C]**	**RMSE [°C]**	**D_{max} [°C]**
Floor	1.3	1.9	1.2	2.3	1.9	2.3
Ceiling	0.7	1.1	0.2	0.7	0.7	0.9
North Wall	0.4	0.9	0.3	0.4	1.2	1.5
West Wall	0.3	0.4	0.3	−0.7	0.5	0.7
East wall	0.3	0.6	0.4	0.5	0.1	−0.1
South Wall	1.4	2.0	0.4	0.6	0.5	0.7

water temperature. This aspect can also be seen in Fig. 9(a), where the temperature difference between surface and supply temperature is reported. This analysis shows that the floor, along with the North and West surfaces, reaches a lower surface temperature value during the cooling tests, which is closer to the supply.

One aspect that emerges from the tests is the air stratification temperature, which can be compared among the different tests (Fig. 9 (b)). The vertical walls lead to very similar stratification values; on the contrary, the cooled ceiling takes to a very uniform air temperature in the room and the vertical gradient is quite zero. The vertical gradient in the case of cooled floor has a relevant value; in the tested conditions, it results being lower than the limit for discomfort given by the Standard ASHRAE 55, whose value of 1.76 K/m corresponds to 3 °C difference between ankle and neck [46]. However, it can be noticed that this value is very close to those obtained from the measurements highlighting a possible critical issue related to floor cooling.

4.2. Results for the modelling approach

This section presents a comparison between the surface and air temperature simulated dynamic profiles with those obtained from measurements. Only the most representative cases are reported, as the large amount of acquired data and simulations performed does not allow the insertion of the whole material in this paper. However, it was decided to show the profiles obtained from simulations of the floor, the ceiling and the North wall. To further compare the two approaches, the root mean square error (RMSE) and the maximum deviation (D_{max}) are calculated for the whole analysed data. The indicators are computed over the operation time of the radiant surface, from the start-up to the shutdown timestep. The RMSE for both surface and air temperatures is defined in Eq. (7):

$$RMSE = \sqrt{\frac{\sum_{t=\tau_1}^{\tau_3} \left(T_s(t) - T_{m,avg}(t)\right)^2}{n_t}} \tag{7}$$

where t denotes the timestep, τ_1 and τ_3 represent respectively the start-up and shutdown timesteps, T_s is the simulated temperature, $T_{m,avg}$ is the average measured temperature, and n_t represents the number of timesteps in the considered interval.

The results of cooling season simulations (Figs. 10–12) show for each test the air and surface temperature profiles for the three phases with continuous lines (simulated profile) and dashed line (experimental data); the supply temperature is also plotted to highlight the switching on of the radiant panel; finally, the global horizontal radiation during the test is plotted (green-dotted line).

In Table 4, the RMSE values are reported together with the maximum deviation for both surface temperature profiles and air temperature. In the calculations, the measured wall and air temperatures are the average values of those detected by the sensors installed on the active surface and on the column, respectively.

From both the plots and the values of RMSE and D_{max}, good ability of the model to reproduce the behaviour of the test room can be assumed; in particular, maximum values of 2.3 °C and 1.9 °C as RMSE for the surface and air, respectively, can be considered acceptable values for the presented analysis.

The results of the experimental campaign performed during the heating season are reported in Figs. 13–15 for the North wall, East wall and the ceiling. In the graphs, the temperature profile obtained from simulations (dashed line) is compared with the measured one (continuous line). Besides the surface temperature, the air temperature is also plotted in the graphs. For both the chosen parameters, it was decided to report the detected temperatures by each sensor and compare them with the simulated profiles.

As seen in the previous figures, the DigiThon model can reproduce the behaviour of the active panel with a good approximation during the heating tests. In Table 5, the calculated RMSE value is reported, and it can be noticed that the highest value is equal to

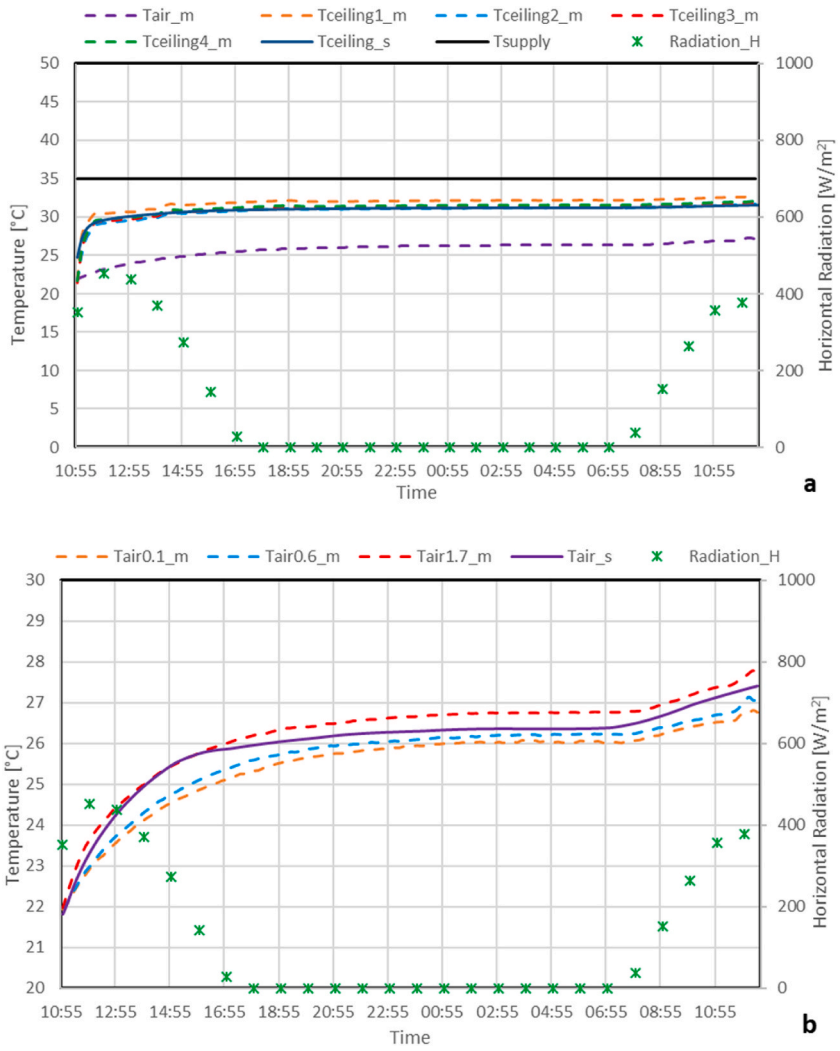

Fig. 13. Surface temperature detected on the active surface (top graph) and air temperature at different heights (bottom graph) compared to simulation outputs in the heating tests for the ceiling.

1.67 °C, which turns into 0.75 °C if only the deviations in air temperatures are considered.

4.3. Discussion

The results presented in the previous section may be used to outline the radiant panel's behaviour further. The different tests changing only a few parameters aim to analyse the impact of single aspects (e.g., different blinds' position, different panel materials and layout) on the outputs presented in this study.

The observation of start-up time and surface gradient temperature (Table 3) shows a close relationship between these parameters: some surfaces need a lower time to reach steady conditions, and this is coupled with a higher surface temperature gradient (e.g., North and West wall); on the contrary, slower surfaces also have a lower gradient (e.g., floor and ceiling). It can be noticed that differences are more relevant considering different panels instead of different tests, suggesting that the different blind position in the tests would have a limited impact on these parameters. However, it is not easy to replicate the same boundary conditions in each test, and it can be concluded that within the limits analysed by this study, the responsiveness of radiant panels is influenced by their composition and layout. As already stated, results show that the North surface is the fastest (the reason can be found in the high pipes density over the surface, with a value of 23.3 m/m^2) and the floor is the slowest (probably for its more massive composition – it is the only surface with embedded tubes).

The layout and composition of panels seem to have an impact also on Delta (Table 3) and $\Delta T_{sur,w}$ (Fig. 9(a)). In particular, surfaces with higher responsiveness (North, West) and higher thermal mass (floor) show a lower temperature difference between the surface and the water supply which is due to a smaller resistance between the panel and the pipe. Moreover, the impact of different tests can be observed: in tests where the blinds are closed (Test C1), the active surface reaches the equilibrium on a lower temperature value,

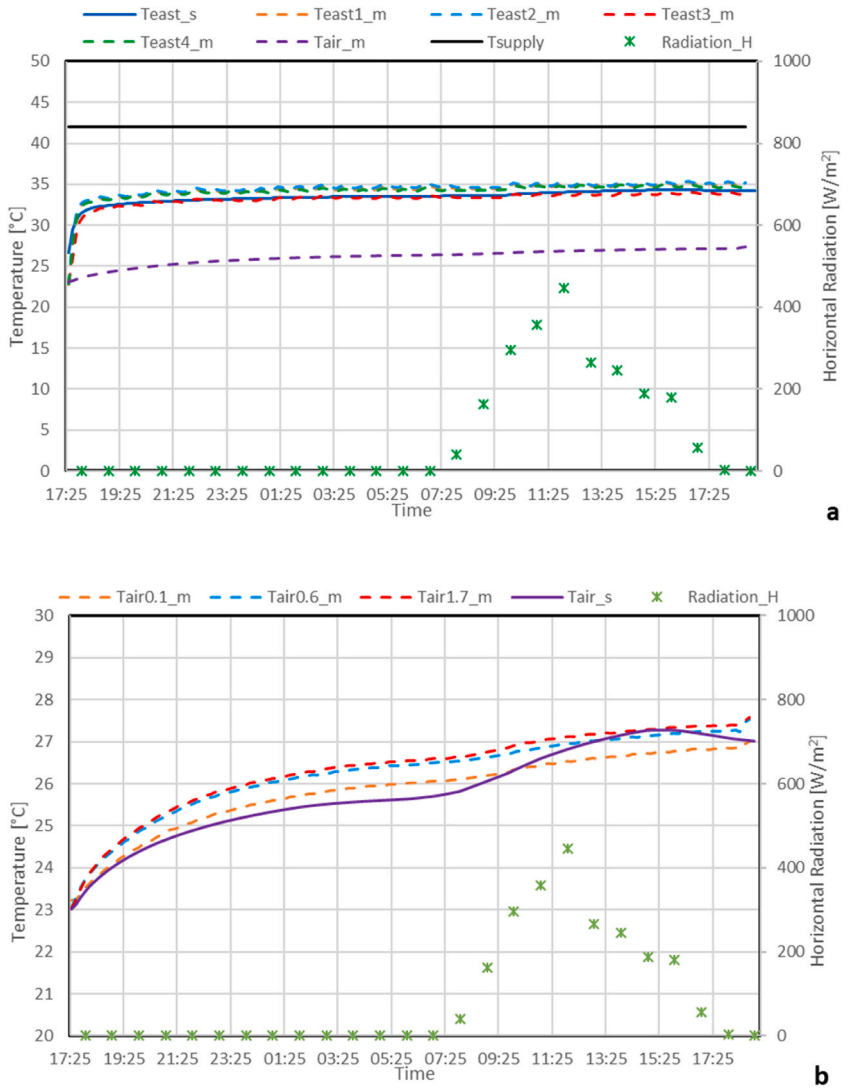

Fig. 14. Surface temperature detected on the active surface (top graph) and air temperature at different heights (bottom graph) compared to simulation outputs in the heating tests for the east wall.

dealing with a lower value of $\Delta T_{sur,w}$ and this aspect can be observed in almost all the cases; on the contrary, in the tests with the presence of the thermal dummy (Test C3), higher surface temperature is detected.

The analysis of radiant surfaces' effect on air temperature (Table 3, but also Figs. 10–12) shows that the floor and the ceiling take to a higher air temperature decrease due to the larger exchange surface. Also, the surface temperature affects this behaviour, which is evident in the floor (with respect to the ceiling) and the North (with respect to the other walls), causing a higher air temperature decrease rate. There is also a slight correlation between the initial temperature of the test and the air gradient: in general, higher loads (solar radiation, internal gains) in Tests C2 and C3 deal with higher initial temperatures, which takes to higher air gradients. It is not possible to compare these values with those emerging from the heating case study, as in that case, the test time is much longer, with a decrease in the air gradient which is very similar for all the surfaces.

In the reported graphs (Figs. 10–12) concerning simulations on cooling tests, the different thermal behaviour of the floor radiant system is visible; it is slower than the ceiling and much slower than the North wall in reaching a steady temperature; however, the DigiThon software can reproduce with good approximation the system's dynamics. In the simulations concerning the North wall, the gap between measurements and simulations is constant and takes to RMSE values between 2.0 and 2.5 °C, with a lower surface temperature in measurements than in simulations.

In the results obtained from the heating tests, it can be observed (Figs. 13–15) that the different sensors detect a close temperature between them, showing a slightly uniform temperature over the active surface. Also the air stratification was one of the observed parameters for these tests; however, the values are lower than those indicated in the ASHRAE 55 Standard for discomfort limits [46] ranging between 0.4 K/m and 1.2 K/m.

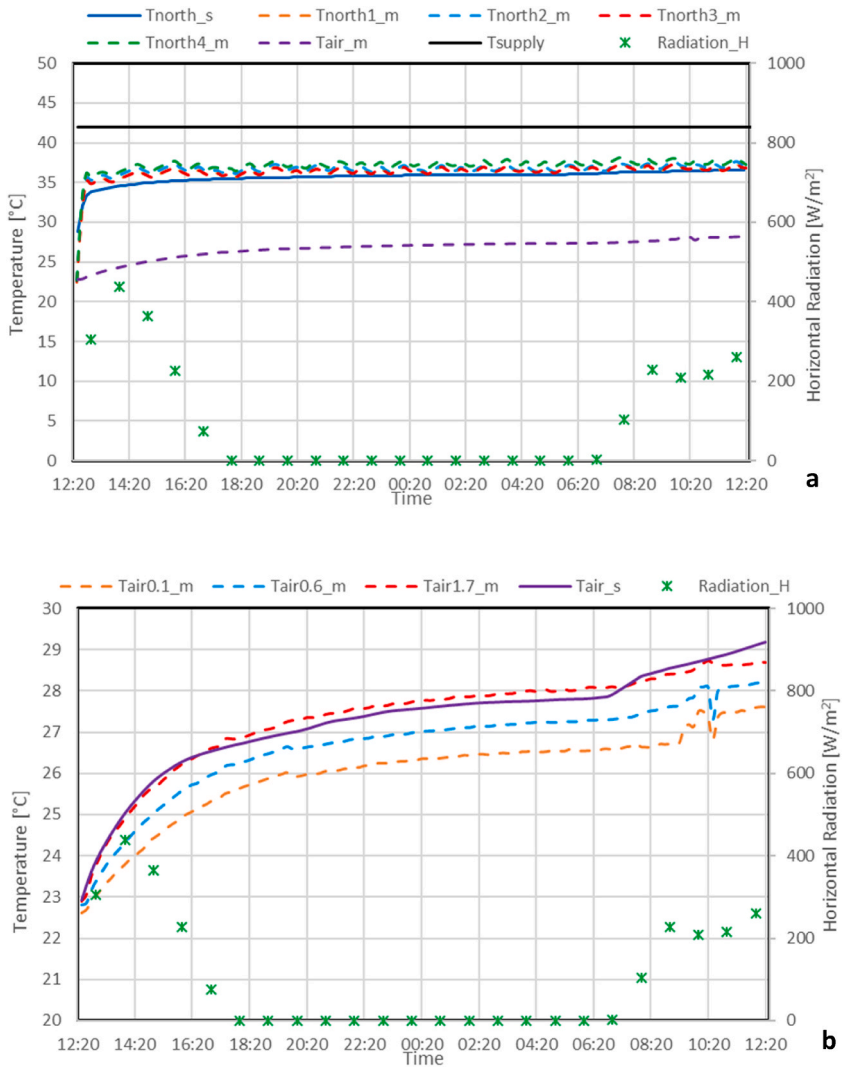

Fig. 15. Surface temperature detected on the active surface (top graph) and air temperature at different heights (bottom graph) compared to simulation outputs in the heating tests for the north wall.

Table 5
RMSE between measurements and simulations for the simulations in heating conditions.

	Ceiling	North Wall	West Wall	East Wall	South Wall
	[°C]	[°C]	[°C]	[°C]	[°C]
Surface temperature	0.41	1.40	0.71	1.25	1.67
Air temperature	0.36	0.41	0.10	0.50	0.75

5. Conclusions

In this paper, the CORE-CARE laboratory equipped with radiant systems has been introduced. Particular experimental measurements have been carried out for the transient thermal assessment of the test room during both heating and cooling seasons. Since its radiant surfaces present different construction features, the dynamic response of each one to different HVAC system settings and boundary conditions has been individually monitored. Based on the collected data, a model of the test room able to consider the different radiant systems was built employing the numerical software DigiThon and the dynamic simulation outputs were compared to real data trends. All tests were performed with one radiant surface turned on at a time considering a working cycle with start-up, steady operation, and shutdown phase. In winter tests water was supplied at temperatures ranging between 35 and 42 °C, and venetian blinds were kept closed. In summer tests water was supplied at 16 °C and three experimental cases were settled: closed blinds, opened blinds and presence of a 180 W thermal dummy. The results of the present paper are closely related to the case study; for this reason, it is not

possible to provide a comparison with previously published papers.

The overall analysis led to the following results:

- In cooling conditions, the start-up times show that the North and West surface exhibit the highest velocity in reaching steady state operation (maximum of 60 min for both), whereas the floor presents the slowest variation profile (maximum of 150 min). The average surface temperature gradients confirm this behaviour, with a decrease rate of at least −10.9 and −9.4 K/h for North and West wall, respectively, and at maximum −5 K/h for floor. The responsiveness is affected by the radiant surface composition and layout, as the North one is composed of lightweight panels with high density of tubes (short pitch), while floor is characterised by a massive structure with relevant thermal inertia.
- In summer, both responsive (North and West) and massive surfaces (floor) manage to bring the wall temperature close to the water supply one, within a difference ranging between 1.5 and 3.5 °C. However, the equilibrium temperature rises in the test with opened blinds (Test C2) and with the presence of the thermal dummy (Test C3).
- Cooled floor has the largest impact on air temperature decrease rate, inducing an average air temperature gradient up to −1.1 K/h. A significant thermal stratification is also observed, with a vertical gradient of about 1.6 K/m, which is close to the limit for discomfort of 1.76 K/m recommended by Standard ASHRAE 55.
- The good agreement between simulations and measured data in the cooling tests suggests that the numerical model is suitable to represents the transient behaviour of the test room. Considering the whole experimental campaign, the largest obtained values of RMSE are 2.3 and 1.9 °C for the North surface and air temperature, respectively.
- In the heating season tests, the active surfaces reach almost a uniform temperature as the sensors positioned in different points gave close measured values. A good agreement between measured data and simulation results is observed, with a maximum RMSE of 1.67 and 0.75 °C for the active surface and the air, respectively, in the test on the South wall.

The thermal assessment of the laboratory carried out through the analysis of collected data and the detailed modelling of the chamber is the first necessary step to acquire the adequate knowledge about the dynamic behaviour of the test room and guarantee the most precise control possible in future tests. The validated numerical model can be used to better design the tests in the laboratory as well as to simulate real rooms. Future works will investigate the impact of other HVAC system aspects, e.g., the operation of the mechanical ventilation unit. Further studies may include tests for analysing the correlation between comfort and people productivity, as well as tests focusing on thermal comfort and causes of localised thermal discomfort.

CRediT authorship contribution statement

Marco Marigo: Conceptualization, Methodology, Software, Data curation, Writing - original draft, Writing - review & editing. **Giacomo Tognon:** Conceptualization, Methodology, Software, Data curation, Data curation, Writing - original draft, Writing - review & editing. **Giulia Alessio:** Conceptualization, Methodology, Software, Data curation. **Michele De Carli:** Supervision. **Angelo Zarrella:** Conceptualization, Methodology, Supervision, Writing – review & editing, Project administration.

Declaration of competing interest

The authors declare that they have no known competing financial interests or personal relationships that could have appeared to influence the work reported in this paper.

Data availability

Data will be made available on request.

Acknowledgements

This work was developed as part of the Project BIRD n.213710, titled “AEOLUS - new criteria for assessing the indoor environmental quAlity to Enhance the well-being of peOpLe their prodUctivity and their Satisfaction” which has received funding from the Department of the Industrial Engineering of the University of Padova.

Appendix A. Wall stratigraphy and material’s thermophysical properties

In this Section, the composition of each wall of the CORE-CARE laboratory is presented. The layout of each wall can be seen in Table A1-A6, together with the thermophysical properties of each material. As the room was built in an existing building, each radiant panel was placed on the pre-existing wall with an additional insulation layer, as it can be noticed in the following tables.

Table A1
Stratigraphy of the floor and materials' thermophysical properties.

FLOOR	Width	Thermal Conductivity	Specific heat	Density
	[m]	[W/(m K)]	[kJ/(kg K)]	[kg/m^3]
Quartzite resin (with embedded radiant system)	0.02	1.31	0.75	2035
Insulation (EPS150)	0.01	0.03	1.34	25
Screed	0.05	1.06	1.00	1700
Concrete	0.05	2.00	0.90	2400
Bricks	0.24	0.57	0.84	900
Plaster	0.01	0.70	0.91	1400

Table A2
Stratigraphy of the south wall and materials' thermophysical properties.

SOUTH WALL	Width	Thermal Conductivity	Specific heat	Density
	[m]	[W/(m K)]	[kJ/(kg K)]	[kg/m^3]
Plasterboard with tubes	0.02	0.25	1.00	820
Insulation (mineral wool)	0.05	0.03	1.03	50
Plaster	0.01	0.70	0.91	1400
Bricks	0.08	0.40	0.84	666
Plaster	0.01	0.70	0.91	1400

Table A3
Stratigraphy of the east wall and materials' thermophysical properties.

EAST WALL	Width	Thermal Conductivity	Specific heat	Density
	[m]	[W/(m K)]	[kJ/(kg K)]	[kg/m^3]
Plasterboard with tubes	0.02	0.21	0.84	760
Insulation (mineral wool)	0.23	0.03	1.03	50
Plaster	0.01	0.70	0.91	1400
Insulation (EPS)	0.04	0.04	1.30	30
Bricks	0.20	2.00	0.90	2400

Table A4
Stratigraphy of the north wall and materials' thermophysical properties.

NORTH WALL	Width	Thermal Conductivity	Specific heat	Density
	[m]	[W/(m K)]	[kJ/(kg K)]	[kg/m^3]
Plasterboard with tubes	0.02	0.20	0.84	760
Insulation (EPS)	0.05	0.03	1.35	17
Plaster	0.01	0.70	0.91	1400
Bricks	0.08	0.40	0.84	666
Plaster	0.01	0.70	0.91	1400

Table A5
Stratigraphy of the west wall and materials' thermophysical properties.

WEST WALL	Width	Thermal Conductivity	Specific heat	Density
	[m]	[W/(m K)]	[kJ/(kg K)]	[kg/m^3]
Plasterboard with tubes	0.02	0.25	1.00	820
Insulation (mineral wool)	0.05	0.03	1.03	50
Plaster	0.01	0.70	0.91	1400
Bricks	0.08	0.40	0.84	666
Plaster	0.01	0.70	0.91	1400

Table A6
Stratigraphy of the ceiling and materials' thermophysical properties.

CEILING	Width	Thermal Conductivity	Specific heat	Density
	[m]	[W/(m K)]	[kJ/(kg K)]	[kg/m^3]
Plasterboard with tubes	0.02	0.25	0.84	760
Insulation (EPS 200)	0.04	0.03	1.30	30
Aluminium foil	0.00	200.00	0.90	2700
Insulation (mineral wool)	0.10	0.03	1.03	50
Plaster	0.01	0.70	0.91	1400
Concrete	0.20	2.00	0.90	2400
Screed	0.05	1.06	1.00	1700
Bituminous foil	0.01	0.17	1.47	1200

References

[1] Y. Geng, W. Ji, B. Lin, Y. Zhu, The impact of thermal environment on occupant IEQ perception and productivity, Build. Environ. 121 (2017) 158–167, https://doi.org/10.1016/j.buildenv.2017.05.022.

[2] W.J. Fisk, Health and productivity gains from better indoor environments and their relationship with building energy efficiency, Annu. Rev. Energy Environ. 25 (2000) 537–566.

[3] C.F. Chen, S. Yilmaz, A.L. Pisello, et al., The impacts of building characteristics, social psychological and cultural factors on indoor environment quality productivity belief, Build. Environ. 185 (2020), 107189, https://doi.org/10.1016/j.buildenv.2020.107189.

[4] T.H. Pedersen, R.E. Hedegaard, K.F. Kristensen, B. Gadgaard, S. Petersen, The effect of including hydronic radiator dynamics in model predictive control of space heating, Energy Build. 183 (2019) 772–784, https://doi.org/10.1016/j.enbuild.2018.11.015.

[5] Eurostat, Energy data 2020 edition: Statistical book. https://ec.europa.eu/eurostat/databrowser/view/ten00124/default/table?lang=en. (accessed January 18, 2023).

[6] A.L. Pisello, I. Pigliautile, M. Andargie, et al., Test rooms to study human comfort in buildings: a review of controlled experiments and facilities, Renew. Sustain. Energy Rev. 149 (2021), 111359, https://doi.org/10.1016/j.rser.2021.111359.

[7] G.A. Ganesh, S.L. Sinha, T.N. Verma, S.K. Dewangan, Investigation of indoor environment quality and factors affecting human comfort: a critical review, Build. Environ. 204 (2021), 108146, https://doi.org/10.1016/j.buildenv.2021.108146.

[8] H. Wu, Y. Wu, X. Sun, J. Liu, Combined effects of acoustic, thermal, and illumination on human perception and performance: a review, Build. Environ. 169 (2020), 106593, https://doi.org/10.1016/j.buildenv.2019.106593.

[9] S. Das, S. Subudhi, A review on different methodologies to study thermal comfort, Int. J. Environ. Sci. Technol. 19 (2022) 2155–2171, https://doi.org/10.1007/s13762-021-03210-8.

[10] L. Arakawa Martins, V. Soebarto, T. Williamson, A systematic review of personal thermal comfort models, Build. Environ. 207 (2022), 108502, https://doi.org/10.1016/j.buildenv.2021.108502.

[11] S. Van Craenendonck, L. Lauriks, C. Vuye, J. Kampen, A review of human thermal comfort experiments in controlled and semi-controlled environments, Renew. Sustain. Energy Rev. 82 (2018) 3365–3378, https://doi.org/10.1016/j.rser.2017.10.053.

[12] R.F. Rupp, N.G. Vásquez, R. Lamberts, A review of human thermal comfort in the built environment, Energy Build. 105 (2015) 178–205, https://doi.org/10.1016/j.enbuild.2015.07.047.

[13] Z. Wang, R. de Dear, M. Luo, B. Lin, Y. He, A. Ghahramani, Y. Zhu, Individual difference in thermal comfort: a literature review, Build. Environ. 138 (2018) 181–193, https://doi.org/10.1016/j.buildenv.2018.04.040.

[14] R. Silva, M. Brett, A.D. Ferreira, C. Serra, T. Jesus, M. Fino, A. Tadeu, Computational fluid dynamics modeling and experimental validation of the thermofluidic performance of climatic chambers, J. Therm. Sci. Eng. Appl. 12 (2020) 1–12, https://doi.org/10.1115/1.4043808.

[15] B. Ramezani, A. Tadeu, T. Jesus, M. Brett, J. Mendes, Evaluation of the thermofluidic performance of climatic chambers: numerical and experimental studies, Fluid 6 (2021), https://doi.org/10.3390/fluids6120433.

[16] J. Dostál, L. Ferkl, Model predictive control of climatic chamber with on-off actuators, IFAC Proc 19 (2014) 4423–4428, https://doi.org/10.3182/20140824-6-za-1003.01571.

[17] P. Riederer, Thermal Room Modeling Adapted To The Test Of HVAC Control Systems, 37, 2001, pp. 777–790.

[18] R. Vidhyashankar, R. Vinze, S. Nagarathinam, V.K. Natrajan, Modelling spatial variations in thermal comfort in indoor open-plan spaces using a whole-building simulation tool, J. Build. Eng. 46 (2022), 103727, https://doi.org/10.1016/j.jobe.2021.103727.

[19] T. Catalina, J. Virgone, F. Kuznik, Evaluation of thermal comfort using combined CFD and experimentation study in a test room equipped with a cooling ceiling, Build. Environ. 44 (2009) 1740–1750, https://doi.org/10.1016/j.buildenv.2008.11.015.

[20] M. Lança, P.J. Coelho, J. Viegas, Numerical simulation of a night cooling strategy in an office room, Energy Build. 252 (2021), https://doi.org/10.1016/j.enbuild.2021.111359.

[21] Q. Dong, S. Li, C. Han, Numerical and experimental study of the effect of solar radiation on thermal comfort in a radiant heating system, J. Build. Eng. 32 (2020), 101497, https://doi.org/10.1016/j.jobe.2020.101497.

[22] M. Bonello, D. Micallef, S.P. Borg, Humidity micro-climate characterisation in indoor environments: a benchmark study, J. Build. Eng. 28 (2020), 101013, https://doi.org/10.1016/j.jobe.2019.101013.

[23] A.S. Derakhtenjani, A.K. Athienitis, A frequency domain transfer function methodology for thermal characterization and design for energy flexibility of zones with radiant systems, Renew. Energy 163 (2021) 1033–1045, https://doi.org/10.1016/j.renene.2020.06.131.

[24] M. Dongellini, V. Ballerini, G.L. Morini, C. Naldi, B. Pulvirenti, E. Rossi di Schio, P. Valdiserri, A new climate chamber for air-source and ground-source heat pump testing based on the Hardware-in-the Loop approach: design and cross validation, J. Build. Eng. 64 (2023), 105661, https://doi.org/10.1016/j.jobe.2022.105661.

[25] M.A. Hassan, O. Abdelaziz, Best practices and recent advances in hydronic radiant cooling systems – Part II: simulation, control, and integration, Energy Build. 224 (2020), 110263, https://doi.org/10.1016/j.enbuild.2020.110263.

[26] J. Shinoda, O.B. Kazanci, S. ichi Tanabe, B.W. Olesen, A review of the surface heat transfer coefficients of radiant heating and cooling systems, Build. Environ. 159 (2019), 106156, https://doi.org/10.1016/j.buildenv.2019.05.034.

[27] A. Koca, Experimental examination of heat transfer coefficients in hydronic radiant wall cooling systems, J. Build. Eng. 60 (2022), 105209, https://doi.org/10.1016/j.jobe.2022.105209.

[28] Y.L. Yuan, X. Zhou, X. Zhang, Experimental study of heat performance on ceiling radiant cooling panel, Procedia Eng. 121 (2015) 2176–2183, https://doi.org/10.1016/j.proeng.2015.09.090.

[29] W. Jin, J. Jing, L. Jia, Z. Wang, The dynamic effect of supply water flow regulation on surface temperature changes of radiant ceiling panel for cooling operation, Sustain. Cities Soc. 52 (2020), 101765, https://doi.org/10.1016/j.scs.2019.101765.

[30] K. Yu, Z. Cao, Y. Liu, Research on the optimization control of the central air-conditioning system in university classroom buildings based on TRNSYS software, Procedia Eng. 205 (2017) 1564–1569, https://doi.org/10.1016/j.proeng.2017.10.261.

[31] G. Yu, Y. Yao, The experimental research on the heating and cooling performance of light floor radiant panels, Procedia Eng. 121 (2015) 1349–1355, https://doi.org/10.1016/j.proeng.2015.09.018.

[32] M. Krajčík, M. Šimko, O. Šikula, D. Szabó, D. Petráš, Thermal performance of a radiant wall heating and cooling system with pipes attached to thermally insulating bricks, Energy Build. 246 (2021), https://doi.org/10.1016/j.enbuild.2021.111122.

[33] M. Ye, A.A. Serageldin, A. Radwan, H. Sato, K. Nagano, Thermal performance of ceiling radiant cooling panel with a segmented and concave surface: laboratory analysis, Appl. Therm. Eng. 196 (2021), 117280, https://doi.org/10.1016/j.applthermaleng.2021.117280.

[34] A.A. Serageldin, M. Ye, A. Radwan, H. Sato, K. Nagano, Numerical investigation of the thermal performance of a radiant ceiling cooling panel with segmented concave surfaces, J. Build. Eng. 42 (2021), 102450, https://doi.org/10.1016/j.jobe.2021.102450.

[35] B. Junasová, M. Krajčík, O. Šikula, M. Arıcı, M. Šimko, Adapting the construction of radiant heating and cooling systems for building retrofit, Energy Build. 268 (2022), https://doi.org/10.1016/j.enbuild.2022.112228.

[36] J. Oravec, O. Šikula, M. Krajčík, M. Arıcı, M. Mohapl, A comparative study on the applicability of six radiant floor, wall, and ceiling heating systems based on thermal performance analysis, J. Build. Eng. 36 (2021), https://doi.org/10.1016/j.jobe.2020.102133.

[37] M. De Carli, M. Scarpa, R. Tomasi, A. Zarrella, DIGITHON: a numerical model for the thermal balance of rooms equipped with radiant systems, Build. Environ. 57 (2012) 126–144, https://doi.org/10.1016/j.buildenv.2012.04.016.

[38] E.C. for Standardization, EN 60751:2022 - Industrial Platinum Resistance Thermometers and Platinum Temperature Sensors, 2022.

[39] M. De Carli, M. Tonon, Effect of modelling solar radiation on the cooling performance of radiant floors, Sol. Energy 85 (2011) 689–712, https://doi.org/10.1016/j.solener.2010.12.012.

[40] M. De Carli, H. Elarga, A. Zarrella, M. Tonon, Evaluation of energy recovery of multiple skin facades: the approach of DIGITHON, Energy Build. 85 (2014) 337–345, https://doi.org/10.1016/j.enbuild.2014.08.049.
[41] E.C. for Standardization, EN 14240:2004 - Ventilation for Buildings — Chilled Beams — Testing and Rating of Passive Chilled Beams, 2004.
[42] G. Mitalas, D. Stephenson, Room thermal response factors, ASHRAE Trans. 73 (1967) 1–10. papers2://publication/uuid/44A1B43E-2C03-4EDA-B82B-5094AA92F0A4.
[43] HEAT2 – Heat transfer in two dimensions – Buildingphysics.com. https://buildingphysics.com/heat2-3/(accessed January 18, 2023).
[44] E.C. for Standardization, EN ISO 6946:2017 - Standards Publication Building Components and Building Elements - Thermal Resistance and Thermal Transmittance - Calculation Methods, 2017.
[45] ARPAV - METEO VENETO. https://www.arpa.veneto.it/previsioni/it/html/meteo_veneto.php (accessed January 18, 2023).
[46] ASHRAE, ASHRAE 55-2013: Thermal Environmental Conditions for Human Occupancy, 2013.